Available online at www.sciencedirect.com
SCIENCE DIRECT®
Physica A 319 (2003) 163–174
PHYSICA A
www.elsevier.com/locate/physa

Computer simulation of bilayer ice: structures and thermodynamics

Jan Slovák[a,*], Hideki Tanaka[a], Kenichiro Koga[b,1], Xiao C. Zeng[c]

[a] *Department of Chemistry, Faculty of Science, Okayama University, 3-1-1 Tsushimanaka, Okayama 700-8530 Japan*
[b] *Department of Chemistry, Baker Laboratory, Cornell University, Ithaca, NY 14853-1301, USA*
[c] *Department of Chemistry and Center for Materials Research and Analysis, University of Nebraska, Lincoln, NE 68588, USA*

Received 5 August 2002

Abstract

A series of molecular dynamics simulations is performed in order to examine in more detail the results of a previous simulation which shows that a thin film of water, when confined to a hydrophobic slit nanopore, freezes into a bilayer ice crystal composed of two layers of hexagonal rings. Three simulations are carried out and each starts with a different initial configuration but has the same number of molecules and the area density. Using a previously introduced solid-like cluster definition, we monitor the dynamic process of crystallization. We find that only in one case the confined water completely freezes into perfect bilayer of ice whereas in other two cases, an imperfect crystalline structure consisting of hexagons of slightly different shapes is observed and this imperfection apparently hinders the growth of perfect bilayer of crystal. After adjusting the area density to match spatial arrangements of molecules, the latter two systems are able to crystallize completely. As a result, we obtain three forms of bilayer crystal differing in the area density and hexagonal rings alignment. Further analyses of these bilayer crystals provide more insightful explanation on the influence of the boundary condition and the simulation-cell size on the diversity of possible crystallographic structures.

PACS: 64.70.Ja; 61.20.Ja

Keywords: Water; Nanopore; Bilayer ice; Thermodynamics of inhomogeneous systems

* Corresponding author. Fax: +81-86-251-7769.
E-mail address: slovak@cc.okayama-u.ac.jp (J. Slovák).

[1] Permanent address: Department of Chemistry, Fukuoka University of Education, Munakata, Fukuoka 811-4192, Japan.

0378-4371/03/$ - see front matter
PII: S0378-4371(02)01384-5

1. Introduction

In addition to a rich phase behavior and large number of crystalline and amorphous structures of bulk water, many interesting structures and phenomena in confined water has been reported [1–4]. The evidence for rich phase behavior of confined water comes mostly from computer simulations and is yet to be confirmed experimentally. Tools of computer simulation have proven very useful to obtain deeper insight into the complex behavior of confined fluids. In particular, computer simulations for water enable us to understand on the molecular level the cooperativity of hydrogen bonding, solvation, and hydrogen bond network rearrangement dynamics. Moreover, computer simulations also allow us to study metastable states of supercooled water (like low density and high density amorphous [5]) under conditions that are either expensive or difficult to achieve in laboratory experiments. Some new phases and new features of metastable water have been found from computer simulations.

Recently, we performed a series of MD simulations of liquid–solid phase transition of confined TIP4P water [6,7] in a narrow slit composed of two parallel hydrophobic walls [1,8,9]. The width of the slit is about one nanometer, just enough to accommodate two layers of water molecules at certain densities. When lowering the temperature of the system at a fixed load (the pressure exerted on a wall by the molecules in the system), the water undergoes a phase transition from liquid to solid phase. It is found [1] that the resulting solid phase is a crystalline ice, namely, a bilayer ice crystal. The structure of the bilayer ice resembles none of the known structures of the ice polymorphs. Nevertheless the ice crystal still retains basic features of bulk ices. For example, every molecule is hydrogen bonded to four nearest-neighbor molecules. Each layer of ice is composed of slightly distorted hexagonal rings (but still very flat compared to those in ice Ih or Ic), and the two layers are completely in registry.

Another simulation was carried out at slightly different conditions, i.e., at constant lateral pressure rather than constant load and that, revealed another kind of phase behavior. On cooling, the water transforms into a bilayer amorphous phase with a perfect network but without long-range order [2]. Recently, we also reported formation of several quasi-one-dimensional solid structure (ice nanotubes) inside of carbon nanotubes [3].

In a previous study [9], we found that starting from various initial liquid configurations (of the same density), we can prepare crystals which differ in density and topology. The observation seems to be related to the use of periodic boundary conditions.

This paper is a complementary study aiming at (i) describing and classifying possible crystal topologies in a more mathematical language, replacing a few not very clear arguments used in Ref. [9], and (ii) discussing the thermodynamics and calculating the normal pressure profile for the system.

2. Simulation and structure analysis

We performed three molecular dynamics (MD) simulations of water confined to a space between two plane parallel structureless walls, at fixed temperature ($T = 253$ K)

and fixed load ($P_z = 1$ GPa). The water molecules interact with each other via TIP4P potential and with the two walls via the 9–3 Lennard–Jones potential. The long-range water–water potential is smoothly truncated at 8.665 Å. The simulation cell is a rectangular prism with lateral dimensions $L_x = 65.01$ Å and $L_y = 65.684$ Å, thus keeping the area density $\rho_A = N/A = N/L_xL_y$ fixed. The confined system consists of a fixed number of water molecules $N = 896$. The distance between the walls, L_z, is about 1 nm. Periodic boundary conditions are imposed in the x and y directions. To generate distinct initial configurations, we use configurations stored during a simulation at $T = 257$ K at which the system is well equilibrated and never shows a tendency towards freezing (at least not within our computer simulation time scale). We select three distinct configurations in the course of simulation, which are separated by a time lag of about 2 ns. For other details see Ref. [9].

Every instantaneous configuration generated in the MD simulation entails a vibrational displacement from a local minimum of the potential energy hypersurface. The potential energy of an instantaneous configuration (hereafter called I-structure) has two contributions: the potential energy of the minimum-energy structure, and the thermal excitations. The minimum-energy structures are referred to as the quenched structures (Q-structures [10–12]) and can be obtained by using the steepest descent method. The Q-structures provide useful information about the structure in configuration space and the geometry of molecular arrangement in solid state.

We characterize the solid state and solid-like regions in terms of hexagonal cells. The hexagonal cell is considered to be an elementary unit of the bilayer crystalline structure. It is composed of a pair of coupled hexagonal rings of hydrogen bonded molecules, i.e., a hexagonal ring in one layer with its counterpart in another.

Hereafter we will refer to our three simulations as S1, S2 and S3. In the course of simulation S1 the system freezes into a crystal composed of 224 hexagonal cells. The crystal appears at about $t = 10.5$ ns and apparently is stable during the next 2.5 ns, only occasionally breaking up few of the hydrogen bonds. The crystallization processes in S2 and S3 are however found to be quite different from that in S1. Quite a large portion of the system crystallizes but the simulations never end up in a complete crystal within the simulation time scale. A closer look at the configurations reveals that the hexagonal cells line up in slightly different directions compared to those in S1 and have slightly different shapes: the hexagons do not have exactly the same inner angles as those in S1. This yields heterogeneity in spatial distribution of molecules or, in other words, a small liquid-like patch somewhere in the middle of the simulation box. If certain number of molecules are removed from or inserted to the liquid-like hole, the process of crystallization would complete successfully. In the case of S2 we observed a crystal composed of 218 hexagonal cells (872 molecules) which seems to be perfectly stable after its formation. In the case of S3, after adding certain number of molecules, we obtained a crystal composed of 228 hexagonal cells (912 molecules) which again is very stable after its formation. For more details on the simulation and discussion we refer our reader to Ref. [9]. Fig. 1 shows how the molecules are arranged in the bilayer crystal (after quenching). The picture corresponds to S2 but looks nearly the same as those in S1 and S3.

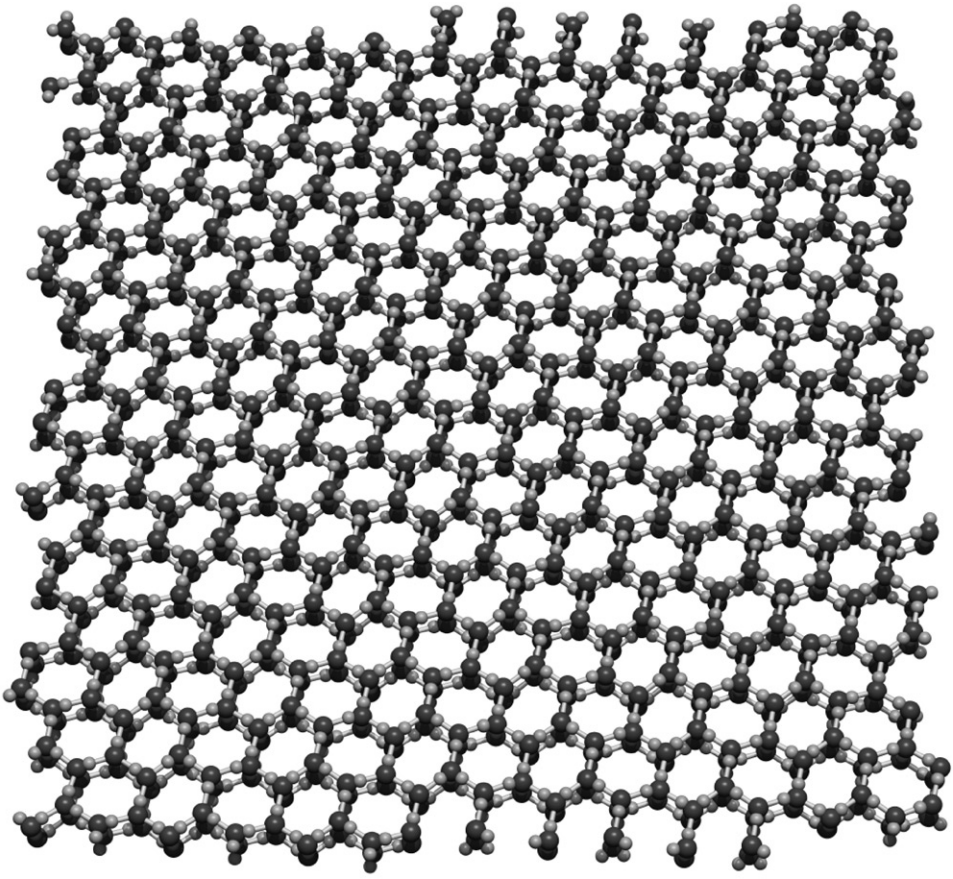

Fig. 1. Typical example of spatial arrangement of molecules in a final configuration in simulation S2.

We generated three bilayer crystals with different densities, each one being perfectly stable. In all three cases the crystal is composed of alternating rows of type-A hexagons and type-B hexagons. The two hexagons differ not only in chirality but also in the inner angles and side lengths. The direction of the rows is also different. But there are always only two types of hexagons. Fig. 2 schematically shows the geometry of the two hexagons. The numerical values of inner angles and side lengths are given in Table 1. The two bilayer-ice rules hold for the crystals: (1) The HOH angle can only be superposed over angles β_A, α_B; (2) when one OH bond of water molecule is normal to the hexagonal lattice plane, the other OH bond can point only along a direction adjacent to the β_A and α_B angle edges. Note also that not every hexagonal ring has the exact shape as depicted in Fig. 2, which is averaged over large number of configurations. All the angles given in Table 1 are within error ± 2 Å and the side lengths within error ± 0.02 Å. The residual entropy of the bilayer ice can be estimated

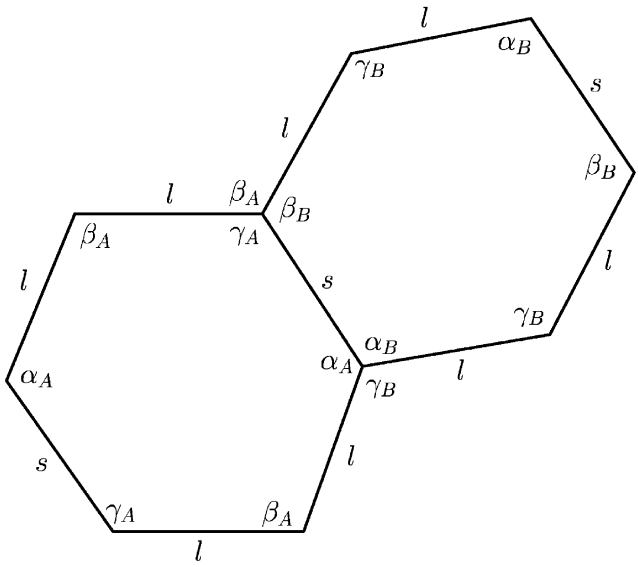

Fig. 2. Geometry of the hexagonal rings in the bilayer ice crystal.

Table 1
Arrangement and geometry of hexagonal rings in a crystal. A and B denote two types of hexagons which generally occur in the resulting structure. l stands for longer sides and s for shorter sides of hexagons

Simulation	α_A	β_A	γ_A	α_B	β_B	γ_B	l	s
I	117.5	108.5	134.5	108.0	117.5	134.5	2.73	2.73
II	112.5	110.0	137.5	115.0	112.5	132.5	2.78	2.75
III	115.5	105.5	139.0	107.5	115.5	137.0	2.72	2.72

with high precision

$$S^{bilayer} = k_B \ln 2^{N/4}\,, \tag{1}$$

where k_B is Boltzmann constant and N number of molecules.

3. Results and discussion

3.1. Periodic boundary conditions

In this section we show that the crystals S1–S3 do differ not only in the density but also in their topology which is clearly dictated by the periodic boundary conditions. Let us illustrate the fact based on the example of S3 structure. Fig. 3(a) shows the xy—projection of the crystal. As we have already mentioned, the structure is composed of alternating rows of hexagons of two types. The solid lines connect the centers of

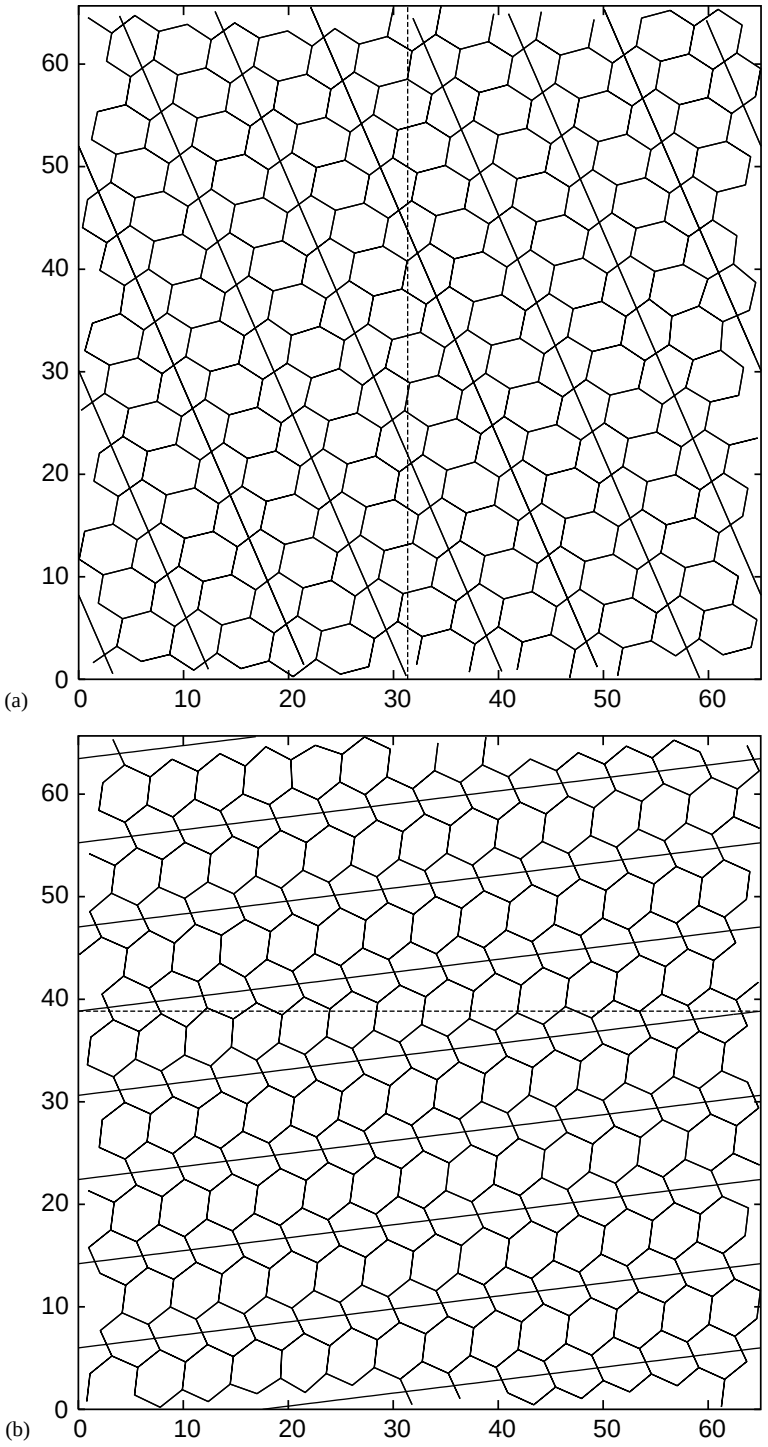

Fig. 3. The final crystalline structure for simulations S3 (a), and S2 (b), (xy projection). The solid lines highlight the rows of hexagons of a specific type. The dashed line connects two subsequent rows.

neighboring hexagons of one type and we can see 8 lines corresponding to 8 rows of the hexagons. Due to the periodic boundary conditions, once a line reaches the right side of the simulation box, it emerges again on the left side, which is depicted by the dashed horizontal line. In this case, the continuation of a line (or its image in the base replica of simulation cell) corresponds to neighboring row of hexagons. But it is a very special case, incidentally. Fig. 3(b) shows the projection of S2 crystal and here the successive solid lines correspond to rows separated by two intermediate rows. The topology of S2 is thus different, S2 and S3 cannot be mapped onto one to another unless the periodic boundary conditions are removed.

Let us express the fact in a mathematical language. The set of lines connecting the centers of hexagons is described by the mapping

$$x \mapsto [X, Y], \quad X = \mathrm{mod}(x, L_x), \quad Y = \mathrm{mod}(ax + b, L_y) \tag{2}$$

of the interval $\langle 0, nL_x \rangle$ into the rectangle $\langle 0, L_x \rangle \times \langle 0, L_y \rangle$, $a \equiv mL_y/nL_x$, m, n are integers, and b is a constant. Actually the above mapping is correct in the case when m, n are comprime numbers. Theoretically m, n need not to be comprime (or the rows can be horizontal or vertical), although none of our three observed structures falls into the special category. In such special cases, mapping (2) is different but what remains true is the fact that a specific topology of a crystalline structure is fully described by two numbers. There is one-to-one correspondence between the pair of numbers $(|m|, n)$ and the topology. The configurations $(m, n), (-m, n)$ are topologically equivalent (with mirror symmetry). The higher one of the two numbers $|m|, n$ has the meaning of the total number of hexagonal rows. For S1, $(m, n) = (4, 7)$, for S2 $(m, n) = (-7, 3)$ and for S3 $(m, n) = (1, 8)$. Each of the three configurations is different. The total number of hexagon rows is either 7 or 8. This is a typical number and it cannot be arbitrary for physical reasons. Although the densities of the crystalline structures differ slightly, they must lie in certain range, too low or too high densities would inevitably lead to the crystal destruction.

The existence of various crystalline structures has at least one unpleasant consequence. In principle, we could extend our simulation algorithm to allow for change of simulation cell, i.e., via scaling of sides and twisting [13] . It would be very useful when looking for the minimal energy structures. The existence of crystals with various densities and hexagon geometry seems unnatural. Unfortunately, due to the existence of topologically non-equivalent structures, we cannot expect the simulations starting with different initial configurations to converge to the same result—single stable crystal with a uniquely defined geometry and lowest potential energy. In this way we could only find the lowest potential energy and geometry corresponding to a crystal with a specific topology.

3.2. Thermodynamics and normal pressure

The computer simulations were performed at constant temperature T, number of molecules N, area $A = L_x L_y$ and load P_z. Here we describe the thermodynamics of the system. The confined system is fully characterized by the variables S, H, A, N, where S

is the entropy and H is the distance between the walls. The corresponding conjugate (intensive) variables are T, P_z, P_x, μ.

The total differential of the internal energy U (variables S, H, A, N)

$$\mathrm{d}U = T\,\mathrm{d}S - AP_z\,\mathrm{d}H - HP_x\,\mathrm{d}A + \mu\,\mathrm{d}N\ . \tag{3}$$

The total differential of the free energy $F \equiv U - TS$ (variables T, H, A, N)

$$\mathrm{d}F = -S\,\mathrm{d}T - AP_z\,\mathrm{d}H - HP_x\,\mathrm{d}A + \mu\,\mathrm{d}N\ . \tag{4}$$

The total differential of the grand potential $\Omega \equiv F - \mu\ N$(variables T, H, A, μ)

$$\mathrm{d}\Omega = -S\,\mathrm{d}T - AP_z\,\mathrm{d}H - HP_x\,\mathrm{d}A - N\,\mathrm{d}\mu\ . \tag{5}$$

Now we can define Gibbs potential $G_1 \equiv F + AHP_x$ (variables T, H, P_x, N)

$$\mathrm{d}G_1 = -S\,\mathrm{d}T - A\Delta P\,\mathrm{d}H + AH\,\mathrm{d}P_x + \mu\,\mathrm{d}N \tag{6}$$

and Gibbs potential $G_2 \equiv F + AHP_z$ (variables T, P_z, A, N)

$$\mathrm{d}G_2 = -S\,\mathrm{d}T + AH\,\mathrm{d}P_z + H\Delta P\,\mathrm{d}A + \mu\,\mathrm{d}N\ , \tag{7}$$

where $\Delta P = P_z - P_x$. It holds

$$\left(\frac{\partial G_1}{\partial N}\right)_{T,H,P_x} = \left(\frac{\partial G_2}{\partial N}\right)_{T,P_z,A} = \mu\ , \tag{8}$$

but only G_1 is homogeneous function of the first order in the variable N, i.e., $G_1 = \mu N$ ($G_2 = \mu N + AH\Delta P$, and $\Omega = -AHP_x$). Apparently, G_2 is the thermodynamic potential corresponding to the simulated system.

Physically, our system is realized as a part of an infinite narrow slit, specified by an area A, whereas the remaining part of the slit plays a role of surrounding reservoir. The system exchanges particles with the reservoir if needed (if μ is fixed rather then N). Thus the physical realization differs from the case in which a finite slit is immersed in a bulk reservoir [14,15]. The bulk reservoir is very convenient when the equilibrium between the bulk and confined liquid is the main objective. The thermodynamic relations in such a system slightly differ from those in the infinite slit [15].

Unlike other inhomogeneous systems in which the grand potential Ω is separated into a bulk and an excess part, and the concept of Gibbs dividing surface is widely used, in the actual realization we can rarely take any advantage of such separation. Generally, the separation is sensible one if some part of the system exhibits bulk properties which is, for example, in the case of a slit immersed in a bulk reservoir, or two bulk phase interface, or a sufficiently wide slit, but not in the case of a very narrow infinite slit. The solvation force f is now defined as

$$f = F/A = -\frac{1}{A}\left(\frac{\partial \Omega}{\partial H}\right)_{T,A,\mu} = P_z\ , \tag{9}$$

i.e., the solvation force is equal to the pressure P_z exerted on a wall by the molecules in the system. This is slightly different from the system opened to the bulk reservoir,

in which the excess grand potential is used in (9) instead of the full grand potential and $f = P_z - p_b$, where p_b is the bulk pressure (outside in the reservoir).

Apart from the load P_z and lateral pressure P_x we can define the pressure tensor $\mathbf{P}$. The pressure tensor is a local quantity and depends on the symmetry of the system. It has two non-zero components, normal pressure p_N and transverse pressure p_T. They are not completely independent as the condition of mechanical stability requires $\nabla\mathbf{P}=0$. Both components are function of the coordinate z perpendicular to the walls.

The interaction potential $v(z,L)$ between molecules of the system and planar walls (located at $z=0$ and $z=L$) can be written as

$$v(z,L) = v_{LJ}(z) + v_{LJ}(L-z)\,, \tag{10}$$

where $v_{LJ}(z)$ is 9-3 Lennard–Jones potential for $z \geqslant 0$ and $v_{LJ} \equiv 0$ for $z < 0$. The relation

$$p'_N(z) = -\rho(z)v'(z) \tag{11}$$

holds for normal pressure. $\rho(z)$ is the density profile of the molecules, which can be calculated from computer simulations. Let $p_N(L/2)$ denote the normal pressure in the middle of the slit and $p_N(0) = p_N(L)$ the pressure on the walls. Then it holds [16]

$$\Delta p_N \equiv p_N(L/2) - p_N(0) = -\int_0^{L/2} \rho(z)v'_{LJ}(z)\,\mathrm{d}z + \int_{L/2}^{L} \rho(z)v'_{LJ}(z)\,\mathrm{d}z\,, \tag{12}$$

whereas the solvation force is

$$f = -\int_0^{L/2} \rho(z)v'_{LJ}(z)\,\mathrm{d}z - \int_{L/2}^{L} \rho(z)v'_{LJ}(z)\,\mathrm{d}z\,. \tag{13}$$

Because we do not know $p_N(0)$ nor $p_N(L/2)$, we can only calculate the normal pressure profile from (11) up to a constant. We set $p_N(L/2) = 0$.

Actually, relation (11) is derived using the T,H,A,μ ensemble and density functional theory. But we performed the simulations at constant T,P_z,A,N which corresponds to a different ensemble. On the other hand, the density profiles obtained from different ensembles at the same thermodynamic conditions must be identical. The calculation of the density profile from the configurations stored during the TP_zAN simulation only requires proper normalization to the correct equilibrium distance L between the walls.

The density profile for the crystal S3 is shown in Fig. 4. The density profiles for S1 and S2 are slightly different, yet hardly distinguishable from the one in Fig. 4. The equilibrium distance between the walls is 9.0474 Å for S2, 9.0673 Å for S1 and 9.0846 Å for S3 crystal, i.e., increasing with increasing area density ρ_A. The peaks are about the same height for all the crystals but they are slightly broadening with increasing density.

If we calculate the solvation force (13) by numerical integration from the density profile, we get $f = 1.0006$ GPa for S3, which is very close to the expected value $P_z = 1$ GPa. If we calculate difference (12) for the same crystal we get 1.0672 GPa. The normal pressure profile is plotted in Fig. 5.

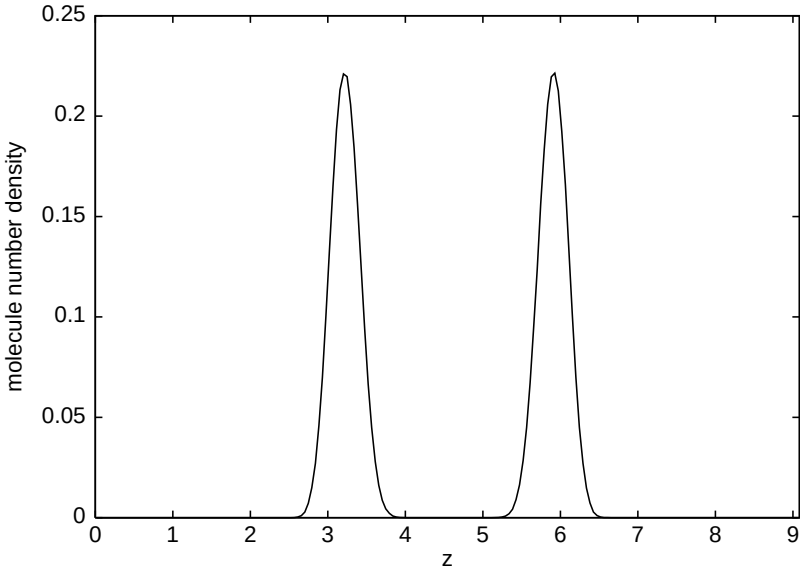

Fig. 4. Density profile of the molecules in the bilayer ice S3 as a function of distance (in Å) from a specific planar wall.

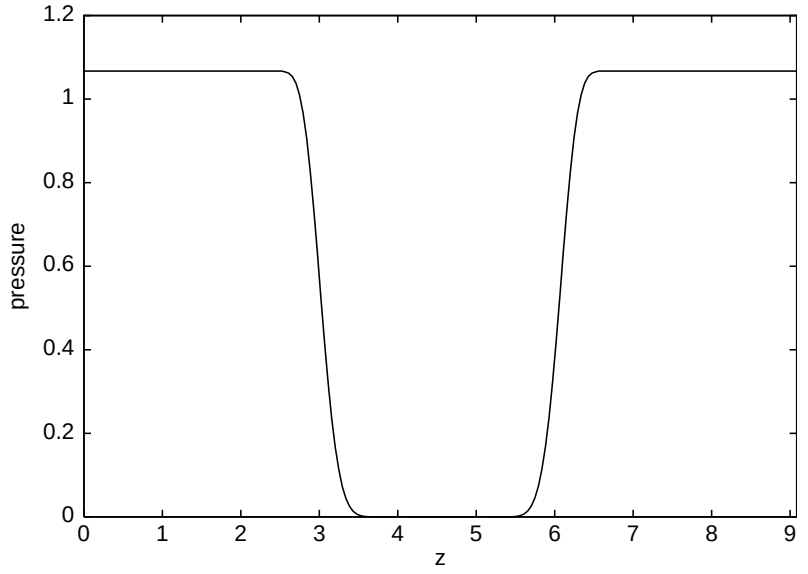

Fig. 5. Normal pressure profile (in GPa) in the bilayer ice S3 as a function of distance (in Å) from a specific planar wall.

The deviation of the numerically calculated solvation force never exceeds 0.5% of the expected value 1 GPa in all three simulations. Considering the fact that the data used to calculate the density profiles were not too extensive (several hundreds configurations at best), it is surprisingly good agreement. The numerically calculated normal pressure profiles look very similar for each of the three crystals and the value Δp_N seems to grow slightly inversely proportionally to the area density. Nevertheless this result should be taken with care as the difference in Δp_N is so small that it can be as well a consequence of poor statistics and limited amount of data available for analysis.

4. Concluding remarks

A series of three MD simulations for a thin film of water confined to a hydrophobic slit is performed in order to examine the influence of the initial configurations, simulation cell size and periodic boundary conditions on crystallization process. At the temperature $T = 253$ K the system freezes and a bilayer ice crystal is formed. The crystal is composed of coupled hexagonal rings, so called hexagonal cells. Generally two types of hexagonal cells can be detected, aligned in alternating rows. The resulting crystals differ in the density and the overall topology. They cannot be mapped onto each to other by any continuous transformation. The topology can be easily described by a pair of integers (m, n).

In order to calculate the normal pressure component of the pressure tensor we discuss first the thermodynamics of the considered system and point out some difference between the system and some similar systems considered so far in literature. The density profile in between the walls is evaluated from computer simulations. We define the solvation force and show that it is equal to the load P_z, i.e., the pressure exerted by the molecules of the system on a wall. The solvation force is estimated by numerical integration from the density profile and compared with the theoretical value. The agreement is excellent, which demonstrates the compatibility of the theory with the computer simulations. The normal pressure as a function of the distance from a wall is not uniquely defined in our case but if the value of normal pressure in the middle of the slit is fixed, the normal pressure profile can be calculated by numerical integration from the density profile. We find out that the three generated crystals differ not only in the topology (which is purely an artifact of periodic boundary conditions) but also in the equilibrium distance in between the walls, in the density profiles and the normal pressure profile, although all these differences are rather tiny.

Acknowledgements

JS and HT are supported by grant-in-aid from JSPS and Ministry of Education and JS is also supported by JSPS post-doctoral fellowship. XCZ is supported by NSF. KK acknowledges the award of JSPS fellowship for Research Abroad.

References

[1] K. Koga, X.C. Zeng, H. Tanaka, Phys. Rev. Lett. 79 (1997) 5262.
[2] K. Koga, H. Tanaka, X.C. Zeng, Nature 408 (2000) 564.
[3] K. Koga, G.T. Gao, H. Tanaka, X.C. Zeng, Nature 412 (2001) 802.
[4] R. Bergman, J. Swenson, Nature 403 (2000) 283.
[5] O. Mishima, H.E. Stanley, Nature 396 (1998) 329.
[6] W.L. Jorgensen, J. Chem. Phys. 77 (1982) 4156.
[7] W.L. Jorgensen, J. Chandrasekhar, J.D. Madura, R.W. Impey, M.L. Klein, J. Chem. Phys. 79 (1983) 926.
[8] J. Slovák, K. Koga, H. Tanaka, X.C. Zeng, Phys. Rev. E 60 (1999) 5833.
[9] J. Slovák, H. Tanaka, K. Koga, X.C. Zeng, Physica A 292 (2001) 87.
[10] F.H. Stillinger, T.A. Weber, J. Phys. Chem. 87 (1983) 2833.
[11] F.H. Stillinger, T.A. Weber, Science 225 (1984) 983.
[12] I. Ohmine, H. Tanaka, P.G. Wolynes, J. Chem. Phys. 89 (1988) 5852.
[13] M. Ferrario, J.P. Ryckaert, Mol. Phys. 54 (1985) 587.
[14] R. Evans, U. Marini Bettolo Marconi, J. Chem. Phys. 86 (1987) 7138.
[15] K. Koga, J. Chem. Phys. 116 (2002) 10 882.
[16] J.R. Henderson, in: D. Henderson (Ed.), Fundamentals of Inhomogeneous Fluids, Marcel Dekker, New York, 1992.